Organic Electronics 30 (2016) 165–170

Contents lists available at ScienceDirect

Organic Electronics

journal homepage: www.elsevier.com/locate/orgel

The enhanced random lasing from dye-doped polymer films with different-sized silver nanoparticles

Shuya Ning [a, b], Zhaoxin Wu [a, *], Hua Dong [a], Lin Ma [a], Bo Jiao [a], Lei Ding [b], Liping Ding [b], Fanghui Zhang [b]

[a] Key Laboratory of Photonics Technology for Information, School of Electronic and Information Engineering, Xi'an Jiaotong University, Xi'an 710049, PR China

[b] College of Science, Shaanxi University of Science and Technology, Xi'an 710021, PR China

ARTICLE INFO

Article history:
Received 7 November 2015
Received in revised form
11 December 2015
Accepted 19 December 2015
Available online 30 December 2015

Keywords:
Organic laser
Localized surface-plasmon resonance
Multiple scattering

ABSTRACT

We reported on the enhanced random lasing from organic dyes doped with silver nanoparticles (Ag NPs), the sizes of Ag NPs ranged from 8 nm to 250 nm. The effects of different sizes of Ag NPs on the lasing properties were studied. We found a strong dependence of the random lasing properties on the size of the Ag NPs, and the lowest threshold was achieved by the introduction of Ag NPs with the diameter of 150 nm. By studying the enhanced localized electromagnetic (EM) field due to localized surface-plasmon resonance and the scattering effect of Ag NPs in experiment and Mie theory, we found that the enhanced localized EM field plays a major role on enhanced lasing of organic dyes for the small Ag NPs (diameter < 50 nm); and the scattering effect is the dominant underlying mechanism for random lasing for the large Ag NPs (diameter ≥ 100 nm), which also suggest that the lowest threshold and strongest lasing are dominated by the photon scattering.

1. Introduction

Recently, metal nanoparticles (NPs) have been widely investigated for the applications in nanolasers [1–5] and optoelectronic devices [6] to biosensors [7]. It had been demonstrated that the coherent and incoherent random lasing of gain media were induced by the golden or silver NPs. Generally speaking, metal NPs enhance the lasing efficiency via two different mechanisms [8]: (i) enhancement of localized electromagnetic (EM) field in the vicinity of metal NP due to localized surface-plasmon resonance (LSPR) [9–11] and (ii) enhancement of the scattering strength, resulted from large scattering cross section of metal NP. As for the gold NPs, Popov et al. studied the enhancement effect of different sizes of gold NPs on the lasing characteristics in a polymer film doped with Rhodamine 6G (Rh6G) [8,12]. T. Zhai et al. showed a threshold reduction for waveguide-plasmonic scheme constructed by coating the gain medium onto gold nanoisland structures [13]. E. Heydari reported the threshold reduction in the gold NP-based random laser by tuning the coupling between the gain material and the LSPR of Au-NPs [14]. In these works, the LSPR spectra of Au NPs overlap sufficiently with emission spectra of the dyes, and photon scattering is expected to be dominant mechanism to enhance lasing properties for Au NPs. As for the Ag NPs, Dice et al. firstly demonstrated an incoherent random laser emission by introducing a suspension of 55 nm-Ag NPs in the solution of Rh6G in 2005 [15]. And then, Meng et al. reported the enhanced emission of coherent random lasing in polymer films by introducing Ag NPs with the diameter of 2 nm and 50 nm respectively [16,17]. And they also discussed the coupling between LSPR of core–shell Ag NPs and organic dyes [18]. In these works, the enhanced localized EM field is considered to be the dominant mechanism, especially for the sizes of Ag NPs below 50 nm. However, Rh6G was used as laser dyes which emission spectrum doesn't overlap with the LSPR spectra of Ag NPs. The deviation between emission spectrum of Rh6G and LSPR spectra of Ag NPs is not optimal for the lasing properties. According to the above works about the Ag NPs, we can know that the present researches are all limited to used several small size Ag NPs (2 nm, 50 nm) to enhanced lasing properties, and the research about the large size Ag NPs ($\geq$100 nm) on lasing properties is absent. Therefore, systematic investigation on the lasing properties affected by Ag NPs of different size with different LSPR is desirable.

Here, we report on the effects of Ag NPs with different sizes on

* Corresponding author.
E-mail address: zhaoxinwu@mail.xjtu.edu.cn (Z. Wu).

http://dx.doi.org/10.1016/j.orgel.2015.12.021
1566-1199/

the lasing properties of organic gain medium. The diameters of Ag NPs ranged from 8 to 250 nm with different LSPR peaks. To this end, different Ag NPs were doped into gain medium, and kept constant the mass concentrations to ensure the same gain volume and enable a more critical examination, and the lowest lasing threshold was achieved by introducing Ag NPs with a diameter of 150 nm. In addition, it was also found that the enhanced localized EM field plays a major role on the enhanced lasing of organic dyes with small Ag NPs (<50 nm); the scattering effect mainly contributes to the enhanced lasing for the large Ag NPs (≥100 nm).

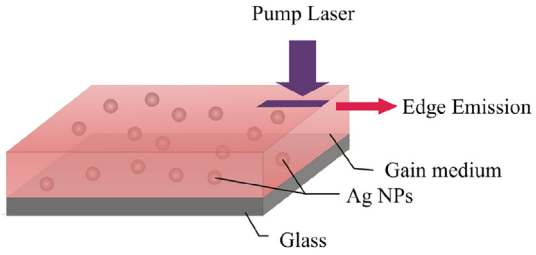

Fig. 2. Schematic illustration of glass/PS: Alq_3: DCJTB doped with Ag NPs.

2. Experiment

Ag NPs having a well-controlled size were synthesized by a seed-mediated growth method [19]. Different sizes of Ag NPs were prepared in two steps by citrate reduction of silver nitrate ($AgNO_3$) with $NaBH_4$ as strong reducing agent in water. First, small Ag NPs were synthesized under chemically reducing $AgNO_3$ in aqueous solution by a rapid nucleation-growth-ripening principle; the resulting Ag NPs were used as starter seeds. And then, slowly adding the proper portions of Ag salt and citrate reducer into the starter seeds solution as obtained in the first step. The slow process ensures aggregation of the released Ag atoms on the Ag nucleation centers without the formation of new centers. In this way, the final sizes of the NPs were tuned, and we prepared NPs with the diameters as: 8, 20, 50, 100, 150, 180, 200 and 250 nm. Fig. 1 shows the Atomic Force Microscopy (AFM) images of Ag NPs with different sizes.

The gain medium was fabricated as follows: Polystyrene (PS), tris(8-hydroxyquinolinato)aluminum (Alq_3) and 4-(dicyanomethylene)-2-tert-butyl-6(1,1,7,7 tetramethyljulolidyl-9-enyl)-4H-pyran (DCJTB) were fully dissolved in chloroform solution (PS: Alq_3: DCJTB = 200:100:3.5, wt%). Different sizes of Ag NPs were doped into the solution maintained a constant mass concentration of 1.28×10^{-3} g/cm^{-3}. The solution was then spin-coated with 1500 rpm spin speed atop of the glass substrate, the device structure is shown in Fig. 2. For comparison, the gain medium without Ag NPs on glass substrate was also fabricated. The thickness of gain medium film is about 420 nm.

In the experiment, the thicknesses of organic gain media layer were measured with Stylus Profiler (Dektak 6M, USA). The absorption and photoluminescence (PL) spectra were obtained by UV–Vis spectrophotometer (HITACHI U-3010, Japan) and Fluorescence Spectrometer (Fluoromax-4 spectrofluometer) respectively. The devices were pumped by the third harmonic of Nd: YAG laser (355 nm, 10 Hz repetition rate, and 25 ps pulse duration). Through a pinhole filter, a slit and a cylindrical lens, the laser beam was formed as a stripe with the size of 5 mm × 1 mm, and was perpendicular to the surface of the devices. Edge emission spectra were measured by Fiber Optic Spectrometer (Ocean Optics SpectraSuite, USB2000). The lasing threshold, peak intensity and the full width at half maximum (FWHM) were measured.

3. Results and discussion

Fig. 3 is the LSPR bands of Ag NPs with different sizes, together with the absorption and emission spectra of Alq_3 and DCJTB. The LSPR bands presented are the absorption spectra of Ag NPs. Alq_3: DCJTB is the gain media which is a typical donor-acceptor lasing system reported in previous published reports [20,21]. Alq_3 is used as donor and DCJTB is used as acceptor, which is the Förster resonance energy transfer system [22–25]. It can be clearly seen that the donor emission, centered around 518 nm, overlaps well with the acceptor absorption peak at 512 nm, enabling efficient resonant energy transfer between the donor and acceptor. In addition, the LSPR bands of different sizes of Ag NPs have difference overlaps with the absorption and emission spectra of the Alq_3 and DCJTB,

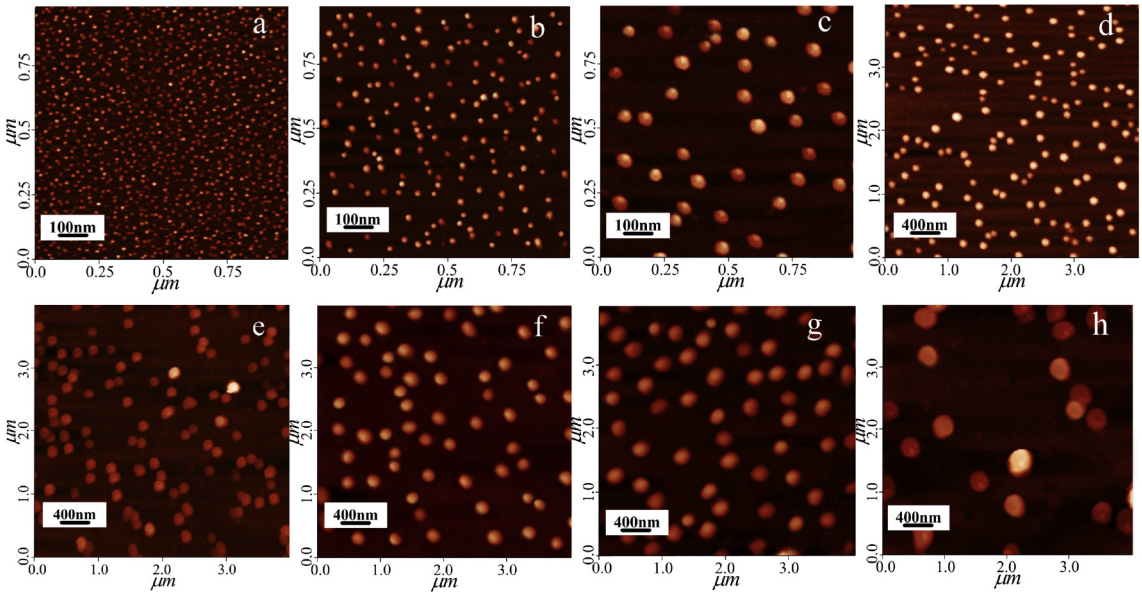

Fig. 1. AFM images of Ag NPs with different sizes. The average sizes of Ag NPs are (a) 8 nm, (b) 20 nm, (c) 50 nm, (d) 100 nm, (e) 150 nm, (f) 180 nm, (g) 200 and (h) 250 nm.

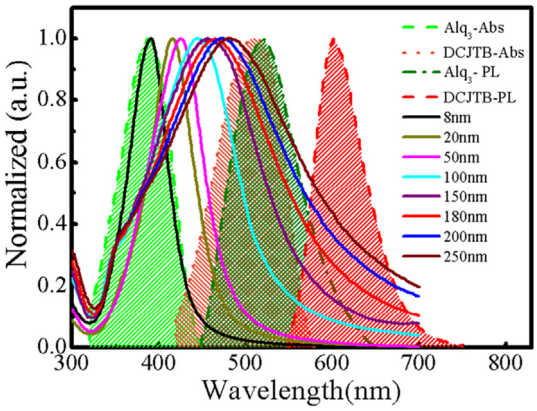

Fig. 3. The LSPR spectra of 8 nm Ag NPs (black line), 20 nm Ag NPs (yellow line), 50 nm Ag NPs (pink line), 100 nm Ag NPs (light blue line), 150 nm Ag NPs (purple line), 180 nm Ag NPs (red line), 200 nm Ag NPs (blue line) and 250 nm Ag NPs (dark red line), together with the absorption and emission of Alq_3 and DCJTB. (For interpretation of the references to color in this figure legend, the reader is referred to the web version of this article.)

which are required for surface plasmon mediated emission enhancement. The LSPR peaks of these Ag NPs show redshift from 389 nm to 475 nm as the diameters of Ag NPs range from 8 nm to 250 nm.

For comparison, the device that gain medium without Ag NPs was prepared as the reference. Fig. 4(a) shows the dependence of edge-emission spectra of the reference device on the pump energy intensity. As described in the previous reports [26–28], the neat gain medium film exhibits an obvious Amplified Spontaneous Emission (ASE) behavior, which only has one peak in the emission spectra. When it is pumped at low energy, it exhibits a broad spontaneous emission spectrum with FWHM of 75 nm. Once the excitation energy becomes large enough, the emission spectrum collapses to a much narrow emission with FWHM of 11 nm. The lasing threshold of 30.1 μJ/cm^2 is then determined shown in the inset of Fig. 4(a). In the reference device, the light is amplified by the gain medium as it propagates along the path of optical gain in a waveguide. Reflections from the internal surfaces can increase the light path length which will build up the ASE. The ASE is light that originates from spontaneous emission and that is subsequently amplified by stimulated emission.

In order to study the effect of different sizes Ag NPs on the lasing characteristics, the lasing thresholds of devices with different sizes of Ag NPs were measured. In the devices with Ag NPs, variation sizes of Ag NPs were maintained a constant mass concentration of 1.28×10^{-3} g/cm^{-3}. Fig. 4(b)–(d) show the edge-emission spectra of the devices with small size Ag NPs (20, 50 nm) and large size Ag NPs (150 nm), respectively. They present the characteristics of coherent random lasing due to the emergence of the sharp spikes in emission spectra. When the excitation energy reaches lasing threshold, the spectrum suddenly becomes narrow, and the FWHM reduces to about 1 nm as the inset of Fig. 4(b)–(d) show. The coherent random lasing comes from the coherent feedback, in those devices, the closed loop paths can be formed through multiple scatterings. These loops could serve as ring cavities for light and the ring cavities are formed by recurrent scattering. When the pump intensity increases, the gain reaches the loss, the laser oscillation occurs in this loop which serves as a laser resonator, and finally laser emission from these resonators results in a number of discrete narrow peaks in the emission spectrum [29,30]. Fig. 4(e) illustrates the laser emission intensity as a function of pump energy for devices with different sizes of Ag NPs. It shows that with the increasing of the Ag NPs size, the lasing threshold reduces at first, and then increases. The lowest lasing threshold of 8.6 μJ/cm^2 is found for the gain medium with 150 nm Ag NPs, about a factor of 3.5 times lower than that of an organic gain medium without any embedded nanoparticles. The trend of lasing threshold is shown in the Fig. 4(f), the thresholds are 25.1, 22.8, 17.3, 12.6, 8.6, 10.8, 11.4 and 13.1 μJ/cm^2 when the diameters of introduced Ag NPs are 8–250 nm, respectively.

As mentioned above, for the device with Ag NPs, there are two main underlying mechanisms to explain these experimental results: (a) Enhancement of localized EM field in the vicinity of metal NPs due to LSPR and (b) Enhancement of scattering strength. In order to determine which mechanism takes effect on the lasing properties and how they work, the devices embedded with TiO_2 NPs which have same scattering strength as that of the corresponding plasmonic Ag NPs had been fabricated. The scattering strength is L/l^*, where L is determined by the laser illumination spot (~5 mm), the mean free path, l^*, can be calculated via Mie theory $l^* = {}^{1}/_{\rho\sigma_s}$, σ_s is the scattering cross section, ρ is number density of nanoparticles. Therefore, a series of different sizes of TiO_2 NPs which have about the same σ_s as that of corresponding Ag NPs and proper ρ were introduced into gain medium, shown in Table 1. Finally, we obtained the devices based TiO_2 NPs having the same scattering strength as that of corresponding Ag NPs. On the condition of same scattering strength, according to compare the lasing threshold of Ag NP-based random laser and TiO_2 NP-based random laser, the contribution mechanism of enhanced EM filed on lasing properties could be known.

The lasing thresholds of devices with different sizes of Ag NPs or TiO_2 NPs are shown in Table 1. We can find that the Ag NP-based random laser described here exhibits superior performance and lower threshold compared to corresponding TiO_2 NP-based random laser. In the Table 1, E_{th}^{ASE} is used to express the ASE threshold of gain medium without Ag NPs; $E_{th\text{-}Ag}$, $E_{th\text{-}TiO2}$ represent the lasing threshold of Ag NP-based random laser and TiO_2 NP-based random laser, respectively; D_{Ag} (D_{TiO2}) is the diameter of Ag NPs (TiO_2 NPs). For the device with Ag NPs, E_{th-Ag}/E_{th}^{ASE} is the ratio of lasing threshold of Ag NP-based random laser to the ASE threshold of reference device, which could show the extent of threshold reduction of the Ag NP-based random laser comparing to the reference device, and reflect the contribution of enhanced localized EM field and scattering effect on lasing properties; Similarly, for the device with TiO_2 NPs, $E_{th-TiO_2}/E_{th}^{ASE}$ is the ratio of lasing threshold of TiO_2 NP-based random laser to the ASE threshold of reference device, which shows the extent of threshold reduction of the TiO_2 NP-based random laser comparing to the reference device, and reflects the contribution of only scattering effect on lasing properties. As shown in Table 1, we can know that, for the devices with small-size Ag NPs (<50 nm), the enhanced localized EM field effect is the major mechanism for enhanced lasing properties. For example, for the device with 8 nm Ag NPs, the $E_{th-Ag}/E_{th}^{ASE} \sim 0.83$, and the corresponding $E_{th-TiO_2}/E_{th}^{ASE} \sim 1$, suggesting that the lasing threshold of TiO_2 NP-based random laser is close to the threshold of reference device, the scattering effect is weak for reducing lasing threshold of TiO_2 NP-based random laser. Due to the same scattering strength between Ag NP-based random laser and corresponding TiO_2 NP-based random laser, we can know that the scattering effect is also weak in the Ag NP-based random laser, then the enhanced localized EM field of Ag NPs plays a main role in reducing lasing threshold; in the same way, for the device with Ag NPs of 50 nm, $E_{th-Ag}/E_{th}^{ASE} \sim 0.57$, the corresponding $E_{th-TiO_2}/E_{th}^{ASE} \sim 0.77$, it is found that the enhancement of localized EM field and scattering has comparable effect; for the case of large-size Ag NPs (≥100 nm), such as 150 nm Ag NPs, $E_{th-Ag}/E_{th}^{ASE} \sim 0.29$, the corresponding $E_{th-TiO_2}/E_{th}^{ASE} \sim 0.47$, which suggests that the

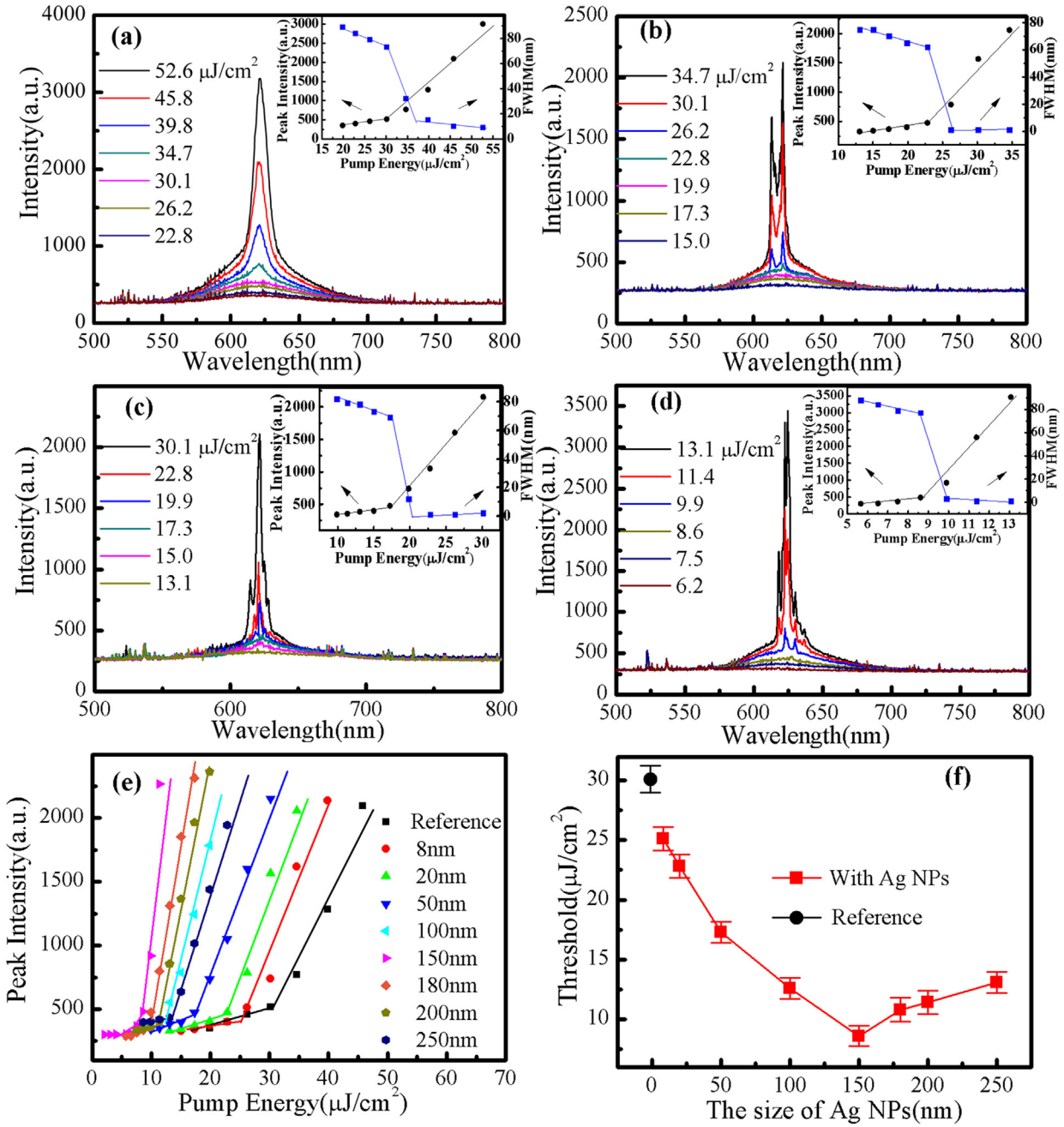

Fig. 4. The emission spectra of the device (a) without Ag NPs; with (b) 20 nm, (c) 50 nm, (d) 150 nm Ag NPs. The insets show the dependence of the lasing intensity and the FWHM of the emission spectra on the pump intensity. (e) Dependences of the emission intensities on the pump energy intensity for the devices. (f) The thresholds for the devices without or with different sizes of Ag NPs. The thresholds are 25.1, 22.8, 17.3, 12.6, 8.6, 10.8, 11.4 and 13.1 μJ/cm^2 when the sizes of Ag NPs are 8, 20, 50, 100, 150, 180, 200 and 250 nm, respectively.

scattering effect is the dominant mechanism for enhanced lasing efficiency. These conclusions for the case of Ag NPs (≤50 nm) are consistent with the results of Meng et al. [16–18].

In order to explore the reason of experiment results above and further identify it, we compare the absorption and scattering cross section of Ag NPs to evaluate the effect of two mechanisms on the lasing properties [15–17]. For the effect of enhanced localized EM field, it is related to the absorption cross section (σ_a) of Ag NPs at $\lambda = 620$ nm. And the scattering effect is related to the scattering cross section (σ_s) of Ag NPs at $\lambda = 620$ nm. Due to the equal mass concentration of Ag NPs with different sizes in the gain medium, $\sigma_a/V_{particle}$ and $\sigma_s/V_{particle}$ were calculated as normalized absorption and scattering cross section to evaluate the mechanism of enhanced random lasing, $V_{particle}$ is the particle volume. Fig. 5(a) presents the dependence of lasing thresholds of the devices with Ag NPs of different sizes. In order to determine the origin of the enhanced lasing properties, two mechanisms are discussed respectively. As for the effect of enhanced localized EM field, the normalized absorption cross section $\sigma_a/V_{particle}$ of different sizes Ag NPs at $\lambda = 620$ nm were calculated by Mie theory [31]. In Fig. 5(b), it shows that with the increase of the Ag NPs size, $\sigma_a/V_{particle}$ increases firstly, and then reduces, there is a maximum of $\sigma_a/V_{particle}$ for the Ag NPs with the diameter of 150 nm at $\lambda = 620$ nm. For the scattering effect, by the Mie theory, the normalized scattering cross section $\sigma_s/$

Table 1
The thresholds of different devices. E_{th}^{ASE} is the ASE threshold of reference device; $E_{th\text{-}Ag}$, $E_{th\text{-}TiO2}$ are the lasing threshold of Ag NP-based device and TiO_2 NP-based device, respectively; D_{Ag} (D_{TiO2}) is the diameter of Ag NPs (TiO_2 NPs). For the device with Ag NPs (TiO_2 NPs), E_{th-Ag}/E_{th}^{ASE} ($E_{th-TiO_2}/E_{th}^{ASE}$) is the ratio of lasing threshold of Ag NP (TiO_2 NP)-based random laser to the ASE threshold of reference device.

Reference	Device with Ag NPs			Device with TiO_2 NPs		
E_{th}^{ASE} (μJ/cm^2)	D_{Ag} (nm)	$E_{th\text{-}Ag}$ (μJ/cm^2)	E_{th-Ag}/E_{th}^{ASE}	D_{TiO2} (nm)	$E_{th\text{-}TiO2}$ (μJ/cm^2)	$E_{th-TiO_2}/E_{th}^{ASE}$
30.1	8	25.1 ± 0.98	0.83	15	29.6 ± 0.91	0.98
30.1	20	22.8 ± 0.98	0.76	35	27.5 ± 0.96	0.91
30.1	50	17.3 ± 0.91	0.57	85	23.1 ± 0.85	0.77
30.1	100	12.6 ± 0.91	0.41	165	19.5 ± 0.94	0.65
30.1	150	8.6 ± 0.88	0.29	240	14.0 ± 0.81	0.47
30.1	180	10.8 ± 0.86	0.36	270	15.1 ± 0.95	0.50
30.1	200	11.4 ± 0.81	0.39	290	15.5 ± 0.88	0.51
30.1	250	13.1 ± 0.81	0.44	345	17.0 ± 0.82	0.55

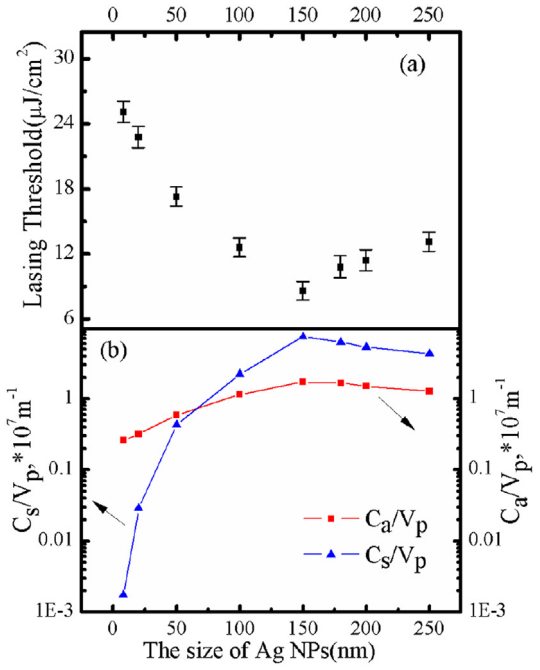

Fig. 5. (a) Lasing thresholds for the devices with different size of Ag NPs. (b) The normalized absorption cross section at λ = 620 nm versus the particle size and the normalized scattering cross section at λ = 620 nm versus the particle size.

$V_{particle}$ of different sizes of Ag NPs at λ = 620 nm were calculated. In Fig. 5(b), it also shows that with the increasing of the Ag NPs size, $\sigma_s/V_{particle}$ increases at first, and then reduces, there is a maximum of $\sigma_s/V_{particle}$ for the Ag NP with the diameter of 150 nm at λ = 620 nm. It also should be emphasized that the normalized scattering cross section $\sigma_s/V_{particle}$ is inversely proportional to the mean free path, l^*, according to the relation $l^* \sim 1/(\sigma_s/V_{particle})$. These allows the evaluation of the scattering strength, L/l^*, which is proportional to $\sigma_s/V_{particle}$. Therefore, the scattering strength has the maximum for the device with 150 nm Ag NPs.

In Fig. 5, for the devices with small-size Ag NPs (<50 nm), the scattering cross section of Ag NPs is much smaller than the absorption cross section, and the thresholds decrease with the increase of $\sigma_a/V_{particle}$ of Ag NPs. Therefore, it implies that the enhanced localized EM field is the dominant mechanism to enhance lasing properties. For the devices with 50 nm Ag NPs, as shown in Fig. 5(b), the effects of localized EM field enhancement and photo scattering are approximately equivalent on reduction of lasing threshold. The results of Ag NPs (≤50 nm) are all consistent with the results of Meng et al. [16–18]. With the increase of particle size (≥100 nm), the scattering intensity of Ag NPs is stronger than the absorption intensity. The scattering effect is the major mechanism for enhanced lasing properties. Furthermore, we can find there is the lowest lasing threshold at the maximum of $\sigma_s/V_{particle}$ of 150 nm Ag NPs, which suggests that the scattering effect plays a main role in the enhancement of lasing properties comparing with enhanced localized EM field. And the conclusion of Fig. 5 is in according with that of Table 1, the result is further confirmed.

4. Conclusion

In summary, we investigated the random lasing based on a series of Ag NPs with the diameter ranging from 8 nm to 250 nm. The effects of different sizes of Ag NPs on the lasing characteristics were investigated. The lowest threshold is achieved by introducing Ag NPs with the diameter of 150 nm. By studying the enhanced localized EM field and the scattering effect of Ag NPs in experiment and Mie theory, we found that the effects of localized EM field enhancement and scattering all contribute to the reduced lasing threshold. As for the small-size particles (<50 nm), enhancement of localized EM field in the vicinity of Ag NPs is the major mechanism for enhanced lasing efficiency; for the large-size particles (≥100 nm), compared with enhanced localized EM field, the scattering effect plays a main role in the enhancement of lasing properties.

Acknowledgments

This work was financially supported by Basic Research Program of China (2013CB328705), National Natural Science Foundation of China (Grant Nos. 61275034, 11574248), Ph.D. Programs Foundation of Ministry of Education of China (Grant No. 20130201110065).

References

[1] M.A. Noginov, G. Zhu, A.M. Belgrave, R. Bakker, V.M. Shalaev, E.E. Narimanov, S. Stout, E. Herz, T. Suteewong, U. Wiesner, Demonstration of a spaser-based nanolaser, Nature 460 (2009) 1110–1113.
[2] D.J. Bergman, M.I. Stockman, Surface plasmon amplification by stimulated emission of radiation: quantum generation of coherent surface plasmons in nanosystems, Phys. Rev. Lett. 90 (2003) 027402.
[3] M.I. Stockman, Spasers explained, Nat. Photonics 2 (2008) 327–329.
[4] L. Dong, F. Ye, A. Chughtai, S. Popov, A.T. Friberg, M. Muhammed, Photostability of lasing process from water solution of rhodamine 6G with gold nanoparticles, Opt. Lett. 37 (2012) 34–36.
[5] R.F. Oulton, V.J. Sorger, T. Zentgraf, L. Dai, G. Bartal, X. Zhang, Plasmon lasers at deep subwavelength scale, Nature 461 (2009) 629–632.
[6] H.A. Atwater, A. Polman, Plasmonics for improved photovoltaic devices, Nat. Mater. 9 (2010) 205–213.
[7] J.N. Anker, W.P. Hall, O. Lyandres, N.C. Shah, J. Zhao, R.P. Van Duyne, Biosensing with plasmonic nanosensors, Nat. Mater. 7 (2008) 442–453.
[8] O. Popov, A. Zilbershtein, D. Davidov, Enhanced amplified emission induced by surface plasmons on gold nanoparticles in polymer film random lasers, Polym. Adv. Technol. 18 (2007) 751–755.

[9] K. Aslan, I. Gryczynski, J. Malicka, E. Matveeva, J.R. Lakowicz, C.D. Geddes, Metal-enhanced fluorescence: an emerging tool in biotechnology, Curr. Opin. Biotechnol. 16 (2005) 55–62.
[10] J.R. Lakowicz, Radiative decay engineering 5: metal-enhanced fuorescence and plasmon emission, Anal. Biochem. 337 (2005) 171–194.
[11] F. Tam, G.P. Goodrich, B.R. Johnson, N.J. Halas, Plasmonic enhancement of molecular fluorescence, Nano Lett. 7 (2007) 496–501.
[12] O. Popov, A. Zilbershtein, D. Davidov, Random lasing form dye-gold nanoparticles in polymer films: enhanced at the surface-plasmon-resonance wavelength, Appl. Phys. Lett. 89 (2006) 191116.
[13] T. Zhai, X. Zhang, Z. Pang, X. Su, H. Liu, Li Wang, Random, Laser based on waveguided plasmonic gain channels, Nano Lett. 11 (2011) 4295–4298.
[14] E. Heydari, R. Flehr, J. Stumpe, Influence of spacer layer on enhancement of nanoplasmon-assisted random lasing, Appl. Phys. Lett. 102 (2013) 133110.
[15] G.D. Dice, S. Mujumdar, A.Y. Elezzab, Plasmonically enhanced diffusive and subdiffusive metal nanoparticles-dye random laser, Appl. Phys. Lett. 86 (2005) 13110.
[16] X. Meng, K. Fujita, Y. Zong, S. Murai, Random lasers with coherent feedback from highly transparent polymer films embedded with silver nanoparticles, Appl. Phys. Lett. 92 (2008) 201112.
[17] X. Meng, K. Fujita, S. Murai, K. Tanaka, Coherent random lasers in weakly scattering polymer films containing silver nanoparticles, Phys. Chem. A 79 (2009) 053817.
[18] X. Meng, K. Fujita, S. Murai, T. Matoba, K. Tanaka, Plasmonically controlled lasing resonance with metallic-dielectric core-shell nanoparticles, Nano Lett. 11 (2011) 1374–1378.
[19] Yu Wan, Zhirui Guo, Xiaoli Jiang, Kun Fang, Quasi-spherical silver nanoparticles: aqueous synthesis and size control by the seed-mediated Lee-Meisel method, J. Colloid Interface Sci. 394 (2013) 263–268.
[20] X.K. Zhao, Z.X. Wu, S.Y. Ning, S.X. Liang, D.W. Wang, X. Hou, Random lasing from granular surface of waveguide with blends of PS and PMMA, Opt. Exp. 19 (2011) 16126.
[21] Wu Lu, Han You, Junfeng Fang, Dongge Ma, Improvement of amplified spontaneous emission performance by doping tris (8-hydroxyquinoline) aluminum (Alq_3) in dye-doped polymer thin films, Appl. Opt. 46 (2007) 2320–2324.
[22] M. Lehnhardt, T. Riedl, T. Weimann, W. Kowalsky, Impact of triplet absorption and triplet-singlet annihilation on the dynamics of optically pumped organic solid-state lasers, Phys. Rev. B 81 (2010) 1652061–1652065.
[23] S. Klinkhammer, X. Liu, K. Huska, Y. Shen, S. Vanderheiden, S. Valouch, C. Vannahme, U. Lemmer, Continuously tunable solution-processed organic semiconductor DFB lasers pumped by laser diode, Opt. Exp. 20 (2012) 6357–6364.
[24] P. Görrn, M. Lehnhardt, W. Kowalsky, T. Riedl, S. Wagner, Elastically tunable self-organized organic lasers, Adv. Mater. 23 (2011) 869–872.
[25] M. Lunz, V.V. Lesnyak, A.L. Bradley, Surface plasmon enhanced energy transfer between donor and acceptor CdTe nanocrystal quantum dot monolayers, Nano Lett. 11 (2011) 3341–3345.
[26] S. Ning, X. Zhao, H. Dong, L. Ma, X. Hou, Enhancement of amplified spontaneous emission in organic gain media by the metallic film, Org. Electron 15 (2014) 2052.
[27] M.A. Díaz-García, F. Hide, M.R. Andersson, Plastic lasers: semiconducting polymers as a new class of solid-state laser materials, Synth. Met. 84 (1997) 455–462.
[28] R. Nedumpara, K. Geetha, V. Dann, C. Vallabhan, P. Radhakrishnan, Light amplification in dye doped polymer films, J. Opt. A Pure Appl. Opt. 9 (2007) 174–179.
[29] C. Vanneste, P. Sebbah, H. Cao, Lasing with resonant feedback in weakly scattering random systems, Phys. Rev. Lett. 98 (2007) 143902.
[30] H. Cao, Review on latest developments in random lasers with coherent feedback, J. Phys. A Math. Gen. 38 (2005) 10497–10535.
[31] C.F. Bohren, D.R. Huffman, Absorption and Scattering of Light by Small Particles, Wiley, New York, 1998, p. 83. Chap. 4.